

Numerical Studies of the Electromagnetic Weibel Instability in Intense Charged Particle Beams with Large Temperature Anisotropy Using the Nonlinear BEST Darwin δf Code*

Edward A. Startsev, Ronald C. Davidson and H. Qin
Plasma Physics Laboratory, Princeton University, Princeton, New Jersey 08543, USA

Abstract

A numerical scheme for the electromagnetic particle simulation of high-intensity charged particle beams has been developed which is a modification of the Darwin model. The Darwin model neglects the transverse induction current in Amperes law and therefore eliminates fast electromagnetic (light) waves from the simulations. The model has been incorporated into the nonlinear δf Beam Equilibrium Stability and Transport (BEST) code. We have applied the model to simulate the transverse electromagnetic Weibel instability in a single-species charged particle beam and the mechanism for nonlinear saturation is identified.

DARWIN MODEL IN PLASMA PHYSICS

It's well known that to describe interacting charged particles one needs to introduce particle phase-space variables (\mathbf{x}, \mathbf{v}) and also independent field phase-space variables which describe the radiation field degrees of freedom. As was shown by Darwin [1], if the particle velocities are small compared to the velocity of light, one can describe particle dynamics correctly up to second order in the small parameter v/c using only the particle phase-space variables (\mathbf{x}, \mathbf{v}) and the Darwin Lagrangian

$$L^D = - \sum_i m_i c^2 \sqrt{1 - \mathbf{v}_i \cdot \mathbf{v}_i / c^2} \quad (1)$$

$$- \sum_{i>j} \frac{e_i e_j}{r_{ij}} \left(1 - \frac{\mathbf{v}_i \cdot \mathbf{v}_j + (\mathbf{v}_i \cdot \mathbf{n}_{ij})(\mathbf{v}_j \cdot \mathbf{n}_{ij})}{2c^2} \right),$$

where the subscript i labels the i 'th particle, $\mathbf{r}_{ij} = \mathbf{r}_i - \mathbf{r}_j$ is the separation between i 'th and j 'th particles, and $\mathbf{n}_{ij} = \mathbf{r}_{ij}/r_{ij}$. The second term in the bracket in Eq. (1) describes corrections of order $(v/c)^2$ to the interaction of the particles. The influence of the independent electromagnetic field on the particle motion is of higher order in the small parameter v/c . Also, the kinetic energy term is usually expanded as $-\sum_i m_i c^2 \sqrt{1 - \mathbf{v}_i \cdot \mathbf{v}_i / c^2} = \sum_i -m_i c^2 + m_i \mathbf{v}_i \cdot \mathbf{v}_i / 2 + m_i (\mathbf{v}_i \cdot \mathbf{v}_i)^2 / 8c^2$ to the same accuracy.

The equivalent description can be obtained with the following single-particle Lagrangian

$$L_i^D = -m_i c^2 \sqrt{1 - \mathbf{v}_i \cdot \mathbf{v}_i / c^2} - e_i \phi + \frac{e_i}{c} \mathbf{A} \cdot \mathbf{v}_i, \quad (2)$$

where the field potentials (ϕ, \mathbf{A}) are determined from the following equations

$$\nabla^2 \phi = -4\pi \rho = -4\pi \sum_{j \neq i} e_j \delta(\mathbf{x} - \mathbf{x}_j), \quad (3)$$

$$\nabla^2 \mathbf{A} + \nabla \psi = -\frac{4\pi}{c} \mathbf{J} = -\frac{4\pi}{c} \sum_{j \neq i} e_j \mathbf{v}_j \delta(\mathbf{x} - \mathbf{x}_j), \quad (4)$$

where $\nabla \cdot \mathbf{A} = 0$. The potential ψ formally solves $\nabla^2 \psi = -(4\pi/c) \nabla \cdot \mathbf{J}$, which removes the longitudinal part of the current \mathbf{J} .

Equations (3) and (4) are Maxwell equations in the Coulomb gauge, neglecting the transverse part of the displacement current $(1/c^2)(\partial^2 \mathbf{A} / \partial t^2)$. If the fields are expanded in Fourier series in time and space according to $\mathbf{A} \sim \exp(-i\omega t + i\mathbf{k} \cdot \mathbf{x})$, neglecting the displacement current is justified whenever $|\omega| \ll |\mathbf{k}|c$ [see Eq. (4)]. Indeed if the oscillation amplitude of the particles is equal to a , then the oscillation frequency is $\omega \sim v_{osc}/a$, where v_{osc} is the average oscillation velocity of the particles. If the distance between two particles is $L \sim 1/k$, then $\omega/kc \sim (v_{osc}/c)/(ka)$. The original Darwin Lagrangian was derived to describe a system of a small number of interacting particles separated on average by a distance $L_D = a \sim 1/k$ from each other. For such a system, the two conditions, $\omega \ll kc$ and $v/c \ll 1$, are equivalent. On the other hand, in plasmas, where $ka \ll 1$, the appropriate condition for the validity of the Darwin model is $\omega \ll kc$, which is much stronger than the condition $v_{osc}/c \ll 1$.

The range of validity of the Darwin model used in the present analysis can be summarized as follows. If there are several species of charged particles in a plasma moving with characteristic average velocity \mathbf{V}_i , then the field created by the particles will be accurately described by Eqs. (3) and (4) provided the condition $|\omega - \mathbf{k} \cdot \mathbf{V}_i| \ll kc$ is satisfied. If we choose one specie to be at rest, and $\omega \ll kc$, then all other species must satisfy $|\mathbf{k} \cdot \mathbf{V}_i| \ll kc$. For example, for the case of a charged particle beam moving through stationary plasma, the beam velocity must be either non-relativistic $V_b \ll c$, or if the beam velocity is relativistic with $V_b \sim c$, then the perturbations must be of the flute type with $k_{\parallel} \ll k_{\perp}$, where (\parallel) and (\perp) are directions parallel and transverse to the direction of beam propagation.

If a beam of radius r_b propagates through low-density background plasma inside a conducting pipe with radius $r_w \sim r_b$, then $k_{\perp} \sim 1/r_b$, and conditions for validity of the

* Research supported by the U. S. Department of Energy

Darwin model are $\omega \ll c/r_b$ and $k_{\parallel}r_b \ll 1$. We estimate $r_b \sim v_{th\perp}/\omega_{\beta}$, where $v_{th\perp}$ is the transverse thermal velocity, and ω_{β} is the transverse smooth-focusing frequency. In this case, the frequencies are limited to $\omega/\omega_{\beta} \ll c/v_{th\perp}$, and the longitudinal wavelengths to $\lambda_{\parallel} \gg r_b$.

In situations where the beam current is completely neutralized by dense background plasma except at the beam edge over a distance comparable to a skin-depth $\delta = c/\omega_{pe}$, we take $k_{\perp} \sim 1/\delta = \omega_{pe}/c$. In this case, the frequencies are limited to $\omega \ll \omega_{pe}$, and the longitudinal wavenumbers to $k_{\parallel} \ll \omega_{pe}/c$. Here, $\omega_{pe} = (4\pi n_p e^2/m_e)^{1/2}$ is the plasma frequency of the background plasma electrons.

NUMERICAL IMPLEMENTATION

In the remainder of this paper, we specialize to the case of a one-component charged particle beam consisting of particles with charge q and rest mass m , in the absence of background plasma. The equations of motion obtained from the Darwin Lagrangian in Eq. (2) contain the time derivative of electromagnetic potential, $\partial\mathbf{A}/\partial t$. This can lead to numerical instabilities when the equations are time-differenced. These difficulties are avoidable if we introduce the canonical momentum $\mathbf{P} = \mathbf{p} + (q/c)\mathbf{A}$ [2]. Specifically, the equations of motion become

$$\frac{d\mathbf{x}}{dt} = \mathbf{v}, \quad (5)$$

$$\frac{d\mathbf{P}}{dt} = \frac{q}{c}\nabla(\mathbf{v} \cdot \mathbf{A}) - q\nabla\phi - m\omega_{\beta}^2\mathbf{x}_{\perp}. \quad (6)$$

Here,

$$\mathbf{v} = \mathbf{p}/m\gamma, \quad \gamma = [1 + (\mathbf{p}/mc)^2]^{1/2}, \quad \mathbf{p} = \mathbf{P} - \frac{q}{c}\mathbf{A}. \quad (7)$$

To calculate the particle trajectories from Eqs. (5) and (6), one needs to determine the electrostatic potential ϕ and the electromagnetic vector potential \mathbf{A} . The Vlasov equation in the new variables can be expressed as

$$\frac{dF}{dt} \equiv \frac{\partial F}{\partial t} + \frac{d\mathbf{x}}{dt} \cdot \frac{\partial F}{\partial \mathbf{x}} + \frac{d\mathbf{P}}{dt} \cdot \frac{\partial F}{\partial \mathbf{P}} = 0, \quad (8)$$

where the characteristics in Eq. (8) are defined by Eqs. (5) and (6). The equation for the electrostatic potential ϕ [Eq. (3)] remains the same, whereas the electromagnetic vector-potential \mathbf{A} is determined by solving a system of coupled equations of the Helmholtz type, i.e.,

$$\left(\nabla^2 - \frac{\omega_p^2}{c^2}\right)\mathbf{A} + \nabla\psi = -\frac{4\pi}{c}\mathbf{J}, \quad (9)$$

where $\nabla \cdot \mathbf{A} = 0$. Here, the factor $\omega_p^2/c^2 = (4\pi n q^2/mc^2) \int d^3P F/\gamma$ arises from introducing the canonical momentum, and the current \mathbf{J} occurring in Eq. (9) is defined by

$$\mathbf{J} = q \int d^3P \frac{\mathbf{P}}{\gamma m} F. \quad (10)$$

For the case of heavy ions with $r_b^2\omega_p^2/c^2 \ll 1$, the skin term can be neglected in Eq. (9), and the above system of equations is linear. For electrons, the skin term is not generally negligible, and the system is nonlinear and is solved by iteration. For a perfectly conducting cylindrical wall with radius r_w , the boundary conditions for ϕ , \mathbf{A} and ψ are especially simple, i.e.,

$$\phi_{r_w} = \mathbf{A}_{r_w} = \psi_{r_w} = 0. \quad (11)$$

The boundary condition for ψ follows from the fact that $\psi = -(1/c)\partial\phi/\partial t$.

To simulate an intense beam which remains close to a known solution to Eq. (3) and Eqs. (8)-(9), it is advantageous to follow the evolution of the small differences ($\delta f, \delta\phi, \delta\mathbf{A}$) between the known solution ($F_0, \phi_0, \mathbf{A}_0$) and the solution of the exact system of equations for $F = F_0 + \delta f$, $\phi = \phi_0 + \delta\phi$, $\mathbf{A} = \mathbf{A}_0 + \delta\mathbf{A}$ [3]. If the known solution is stationary in time ($\partial/\partial t = 0$), the perturbed distribution is determined from

$$\frac{d\delta f}{dt} = -\frac{d\mathbf{x}}{dt}\Big|_{\delta} \cdot \frac{\partial F_0}{\partial \mathbf{x}} - \frac{d\mathbf{P}}{dt}\Big|_{\delta} \cdot \frac{\partial F_0}{\partial \mathbf{P}}, \quad (12)$$

where $|_{\delta}$ denotes the perturbed particle trajectories obtained by using the perturbed potentials $\delta\phi$ and $\delta\mathbf{A}$.

In the particle simulations using the modified BEST code [4], the perturbed $\delta f(\mathbf{x}, \mathbf{p}, t)$ is given by,

$$\delta f = \sum_{i=1}^N w_i \delta(\mathbf{x} - \mathbf{x}_i) \delta(\mathbf{P} - \mathbf{P}_i). \quad (13)$$

where the weight $w = \delta f/F$ solves

$$\frac{dw}{dt} = (1-w) \frac{1}{F_0} \frac{d\delta f}{dt}. \quad (14)$$

Here, N is total number of particles in the simulation. In this approach the noise introduced by such a sampling is also proportional to the weights carried by the particles, and is much smaller than the noise introduced by sampling the original particle distribution F (when $w \ll 1$) by a factor $\epsilon_{\delta f}/\epsilon_F = \bar{w}$. In addition, this δf method can be used to study linear stability properties, provided all nonlinear terms in the dynamical equations of motion are neglected.

SIMULATION RESULTS

The electromagnetic aspects of the BEST code has been benchmarked by comparing with the linear eigenmode code bEASt [5] by simulating the electromagnetic Weibel instability [6] in charged particle beams with large temperature anisotropy $T_{\parallel}/T_{\perp} \ll 1$ and axis-symmetric perturbations with $\partial/\partial\theta = 0$ [7]. We present here some typical numerical results. Our previous numerical studies using the eigenmode code bEASt have shown [5] that the growth rates are insensitive to the normalized skin depth provided $c/r_b\hat{\omega}_{pb} \gg 1$ and that the growth rates are insensitive to

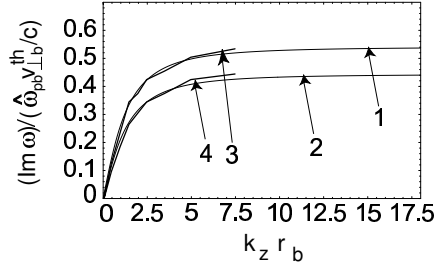


Figure 1: The normalized growth rate $(Im\omega)/(\bar{\omega}_{pb}v_{\perp b}^{th}/c)$ of the Weibel instability is plotted versus $k_z r_b$. Here, $\bar{\omega}_{pb}$ is the on-axis beam plasma frequency.

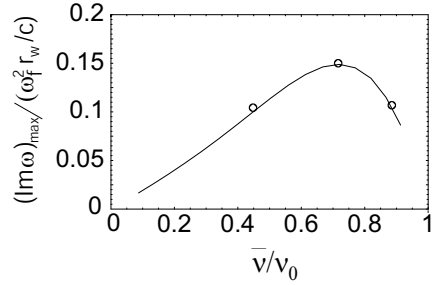


Figure 2: Plot of the normalized maximum growth rate $(Im\omega)_{max}/(\omega_f^2 r_w/c)$ of the Weibel instability versus the average depressed tune \bar{v}/v_0 .

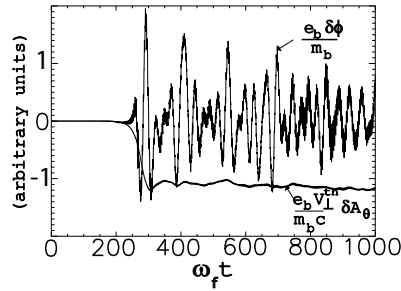


Figure 3: Time history of the electrostatic potential $e_b\delta\phi/m_b$ and azimuthal component of the vector potential $e_b v_{\perp}^{th}\delta A_{\theta}/m_b c$ are plotted versus time [5].

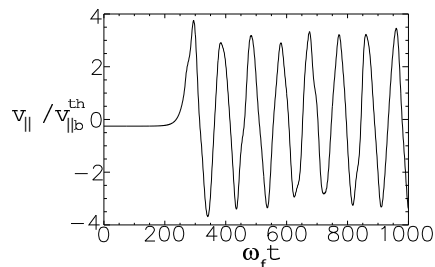


Figure 4: The normalized parallel velocity $v_{||}/v_{||b}^{th}$ of a test particle is plotted as a function of time [5].

the temperature ratio provided $T_{||b}/T_{\perp b} \ll r_b^2 \bar{\omega}_{pb}^2/c^2 \sim (v_{\perp b}^{th}/c)^2$. Therefore, the parameters in the simulations using the BEST Darwin code were chosen so that these conditions apply, with $c/r_b \bar{\omega}_{pb} = 10$ and $T_{||b}/T_{\perp b} = 10^{-6}$. Also, sufficiently intense beams ($\bar{v}/v_0 < 0.82$) with large temperature anisotropy are electrostatically unstable [8]. This electrostatic Harris instability is fast and saturates at moderate values of $T_{||b}/T_{\perp b}$, where the Weibel instability is absent. Therefore, in linear δf simulations with $\bar{v}/v_0 < 0.82$, we have suppressed the electrostatic component of the potential, to only see the Weibel instability. This is possible because the electromagnetic A_{θ} component is decoupled from electrostatic ϕ component.

Figure 1 shows plots of the normalized growth rate $(Im\omega)/(\bar{\omega}_{pb}v_{\perp b}^{th}/c)$ versus $k_z r_b$ obtained for two values of the normalized depressed tune $\bar{v}/v_0 = 0.4(1), 0.72(2)$. Also shown are the results of a linear δf simulation using the Darwin BEST code [$\bar{v}/v_0 = 0.4(3), 0.72(4)$]. Plots of the normalized maximum growth rate $(Im\omega)_{max}/(\omega_f^2 r_w/c)$ versus the average depressed tune \bar{v}/v_0 obtained using the bEAST code are shown in Fig. 2. The dots are the results of linear simulations using the Darwin BEST code. The results obtained using both codes are in good agreement. The nonlinear stage is illustrated in Figs. 3 and 4 for a beam with $\bar{v}/v_0 = 0.88$, where the electrostatic Harris instability is absent. Figure 3 shows the time history of the electrostatic potential $e_b\delta\phi/m_b$ and the azimuthal component of the vector potential $e_b v_{\perp}^{th}\delta A_{\theta}/m_b c$ [5]. At saturation, both have similar normalized amplitudes. Figure 4 shows the normalized parallel velocity $v_{||}/v_{||b}^{th}$ of an individual test particle as a function of time [5]. One can see clearly that the particle motion becomes trapped when the instability saturates. It is found that the particle bounce frequency at saturation is approximately equal to the maximum linear growth rate $(Im\omega)_{max}/\omega_B \approx 0.4$ [9]. In addition, the velocity amplitude at saturation is also proportional to the linear growth rate $v_{osc} \approx (Im\omega)_{max} r_b \sim 3v_{||b}^{th}$ [see Fig. 4].

REFERENCES

- [1] C. G. Darwin, *Phil. Mag.* **39**, 357 (1920).
- [2] C. W. Nielson, H. R. Lewis, *Methods in Computational Physics*, vol. 16, *Academic Press, New York*, 1976, p.976.
- [3] S. E. Parker and W. W. Lee, *Phys. Fluids* **B 5**, 77 (1993).
- [4] H. Qin, R. C. Davidson and W. W. Lee, *Phys. Rev. ST Accel. Beams* **3**, 084401 (2000); **3**, 109901 (2000).
- [5] E. A. Startsev, R. C. Davidson and H. Qin, *Phys. Plasmas* **14**, 056705 (2007).
- [6] E. S. Weibel, *Phys. Rev. Lett.* **2**, 83 (1959).
- [7] E. A. Startsev and R. C. Davidson, *Physics of Plasmas* **10**, 4829 (2003).
- [8] E. A. Startsev, R. C. Davidson and H. Qin, *Phys. Rev. ST Accel. Beams* **6**, 084401 (2003).
- [9] R. C. Davidson, D. A. Hammer, I. Haber and C. E. Wagner, *Phys. Fluids* **15**, 317 (1972).